

# Tunable resonant $s - p$ mixing of excitons in van der Waals heterostructures

Jiayu David Cao,<sup>\*</sup> Konstantin S. Denisov, and Igor Žutić<sup>†</sup>

Department of Physics, University at Buffalo, State University of New York, Buffalo, New York 14260, USA

(Dated: March 18, 2025)

Excitonic states of tightly-bound electron-hole pairs dominate the optical response in a growing class of two-dimensional (2D) materials and their van der Waals (vdW) heterostructures. In transition metal dichalcogenides (TMDs) a useful guidance for the excitonic spectrum is the analogy with the states in the 2D hydrogen atom. From our symmetry analysis and solving the Bethe-Salpeter equations we find a much richer picture for excitons and predict their tunable resonant  $s - p$  mixing. The resonance is attained when the subband splitting matches the energy difference between the  $1s$  and  $2p_+$  (or  $2p_-$ ) excitons, resulting in the anticrossing of the spectral lines in the absorption as a function of the subband splitting. By focusing on TMDs modified by magnetic proximity, and gated 3R-stacked bilayer TMD, we corroborate the feasibility of such tunable spin splitting. The resulting tunable and bright  $s - p$  excitons provide unexplored opportunities for their manipulation and enable optical detection of Rashba or interlayer coupling in vdW heterostructures.

Two-dimensional (2D) materials with their suppressed screening and enhanced Coulomb interactions provide a versatile platform to study excitons with large binding energies [1–10]. The interplay between the Coulomb interaction, multiple valleys, and intrinsic spin-orbit coupling (SOC) in 2D materials influences the excitonic states and the resulting optical response [11]. The sensitivity of excitonic properties to the neighboring regions in their heterostructures offers an important probe for proximitized materials [12]. The transformation of excitons by magnetic, spin-orbit coupling, or charge-density wave proximity effects, as well as by the change in the band topology, or in twisted multilayers [13–22], then becomes a valuable fingerprint for emergent phenomena [23–25].

Transition-metal dichalcogenides (TMDs) [1], one of the most studied 2D materials, offer a useful guidance for the excitonic spectrum from a 2D hydrogen atom, classified by the principal and angular quantum numbers. For a simple isotropic spectrum, the Rydberg-like series,  $1s, 2s, 2p \dots$ , implies that  $s$ -excitons are optically active under single-photon processes. Beyond the simple isotropic two-band model, by adding other discrete degrees of freedom, such as valley or subband (spin or layer), the excitonic wave function acquires admixtures of different angular states resulting, for example, in a partial brightening of  $p$ -like excitons [25–30].

In this work we develop a theory of the resonant  $s - p$  mixing of excitons and an enhanced brightening of  $2p$  states in van der Waals (vdW) heterostructures with tunable subband splittings. We illustrate the idea in Fig. 1 for a monolayer (ML) TMD and excitons formed by spin-up ( $\uparrow$ ) holes ( $A$  excitons) in the  $K$  valley. From Rashba SOC there is a mixing between  $|1s\uparrow\uparrow\rangle$  and  $|2p_+\uparrow\downarrow\rangle$  excitons, the first (second) spin is for hole (electron) from valence (v) [conduction (c)] band, due to the subband spin mixing in the  $c$  band. By including magnetic proximity effect, we change the  $c$  band splitting to push the energy

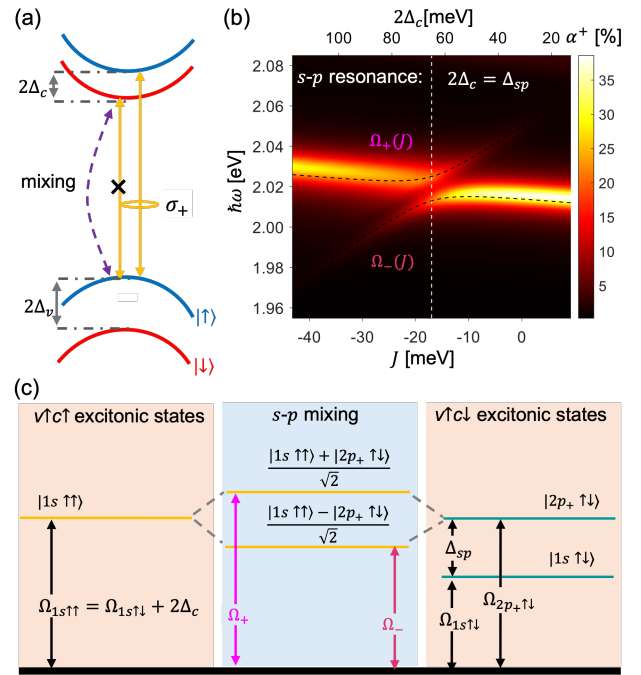


FIG. 1. (a) Schematic of spin-forbidden and spin-allowed optical transitions in the  $K$  valley of proximitized ML-TMDs, with valence (v) and conduction (c) band splitting,  $2\Delta_v \gg 2\Delta_c$ . The mixing is introduced by a broken mirror symmetry. (b) The evolution of the optical absorption as  $2\Delta_c$  is tuned by the proximity-induced exchange coupling  $J$ , calculated by solving the Bethe-Salpeter equation. (c) Exciton energy levels before and after “turn on” the mixing. Yellow (green) lines: bright (dark) excitons. The  $s - p$  resonance condition  $\Omega_{\uparrow\uparrow 1s} = \Omega_{\downarrow\uparrow 2p_+}$  or, equivalently,  $2\Delta_c = \Delta_{sp}$  is demonstrated.

of  $|2p_+\uparrow\downarrow\rangle$  exciton close to that of  $|1s\uparrow\uparrow\rangle$  [Fig. 1(c)]. We achieve a resonant  $s - p$  mixing of excitons, a regime not accessible in intrinsic 2D insulators. The resulting anti-crossing  $s - p$  exciton doublet [Fig. 1(b)] enhances the brightening of  $p$  states, instead of making them weakly active due to remote band admixtures [25–29, 31].

<sup>\*</sup> jiayuc@buffalo.edu

<sup>†</sup> zigor@buffalo.edu

Our analysis uses the massive Dirac electron model with tunable subband splitting, complemented with solving the the Bethe-Salpeter equation (BSE) [32, 33], for magnetically-proximitized TMDs and for nonmagnetic bilayer (BL) TMDs with the gate-voltage controlled top (t) bottom (b) layer splitting. For the two coupled massive Dirac electrons the Hamiltonian is

$$H = \begin{pmatrix} \Delta + \Delta_c & \hbar v_F k_- & 0 & 0 \\ \hbar v_F k_+ & -\Delta + \Delta_v & \gamma^* & 0 \\ 0 & \gamma & \Delta - \Delta_c & \hbar v_F k_- \\ 0 & 0 & \hbar v_F k_+ & -\Delta - \Delta_v \end{pmatrix}, \quad (1)$$

where  $\Delta_{c,v}$  describe the subband splittings in  $c, v$  bands,  $2\Delta$  is the energy gap, and  $v_F$  the Fermi velocity. The intersubband coupling due to broken out-of-plane mirror-symmetry, in the the lowest order of  $k$ , is given by a parameter  $\gamma$ . The basis of  $H$  is  $|c\uparrow\rangle, |v\uparrow\rangle, |c\downarrow\rangle, |v\downarrow\rangle$ . These spins correspond to the real spin for ML-TMDs, or to the t/b-layer index for 3R-stacked BL-TMDs.

The interband transitions in  $H$  are induced by  $\sigma_+$  polarized photons, the time-reversal version of  $H$  is used for  $K'$ -valley which couples to  $\sigma_-$ , with the spin allowed (forbidden) transitions optically active (inactive). To demonstrate the appearance of the  $s-p$  mixing, we use the effective mass approximation (EMA) in the limit of large  $\Delta$ .  $H$  from Eq. (1) will then be used only in BSE. Applying the downfolding procedure [34] in the second-order with respect to e-h ( $c-v$ ) coupling,  $\hbar v_F k / \Delta$ , we arrive at the effective  $2 \times 2$  Hamiltonian for  $c$  and  $v$  bands

$$H_{c(v)} = \pm \left( \Delta + \frac{\hbar^2 k^2}{2m} \right) + \Delta_{c(v)} \sigma_z \pm (\alpha k_- \sigma_+ + c.c.), \quad (2)$$

where  $\boldsymbol{\sigma}$  is the vector of Pauli matrices for subbands,  $\sigma_{\pm} = (\sigma_x \pm i\sigma_y)/2$ ,  $m = \Delta/v_F^2$  is the effective mass, and  $\alpha = \gamma \hbar v_F / (2\Delta)$  is an effective subbands coupling strength. After downfolding the last term depends linearly on  $k$ , unlike  $k$ -independent  $\gamma$  in  $H$ .  $\Delta$  and  $\Delta_{c(v)}$  in Eq. (2) are renormalized by a small  $\gamma^2/\Delta$ .

The exciton wave function in the state  $|S\rangle$  is written as a vector:  $\vec{\Psi}^S(\mathbf{r}) = [\psi_{\uparrow\uparrow}^S(\mathbf{r}), \psi_{\uparrow\downarrow}^S(\mathbf{r}), \psi_{\downarrow\uparrow}^S(\mathbf{r}), \psi_{\downarrow\downarrow}^S(\mathbf{r})]^T$ , in the basis  $|s_v s_c\rangle$ , where the  $s_{v(c)}$  run over subband indices ( $\uparrow, \downarrow$ ) of the  $c(v)$  bands, respectively, and  $\mathbf{r}$  is the electron-hole (e-h) relative motion coordinate. The Schrödinger equation for  $\vec{\Psi}^S(\mathbf{r})$  is

$$[I \otimes H_c(\mathbf{r}) - H_v^*(\mathbf{r}) \otimes I + V(r)] \vec{\Psi}^S(\mathbf{r}) = \Omega_S \vec{\Psi}^S(\mathbf{r}), \quad (3)$$

where  $I$  is the  $2 \times 2$  unit matrix,  $H_{c,v}(\mathbf{r})$  is obtained by  $k_{x,y} \rightarrow -i\partial_{x,y}$  in Eq. (2),  $V(r)$  models the attractive screened Coulomb interaction, and  $\Omega_S$  is the exciton energy. The matrix element of the  $\sigma_+$  polarized optical transition from a ground state  $|0\rangle$  to  $|S\rangle$  described by  $\vec{\Psi}^S(\mathbf{r})$  is given by [35, 36]

$$\langle S | \sigma_+ | 0 \rangle = v_F [\psi_{\uparrow\uparrow}^S(\mathbf{r} \rightarrow 0) + \psi_{\downarrow\downarrow}^S(\mathbf{r} \rightarrow 0)], \quad (4)$$

valid also for  $\alpha \neq 0$ . This expression (i) is nonzero for spin-allowed components of  $\vec{\Psi}^S$  and (ii) accounts for the

probability of finding electron and hole with the same spin at the same point in space ( $\mathbf{r} \rightarrow 0$ ), which is nonzero only for  $s$ -like states. The overall probability of the optical transition is determined by  $|\psi_{\uparrow\uparrow} + \psi_{\downarrow\downarrow}|^2$ , rather than by the sum of separate probabilities,  $|\psi_{\uparrow\uparrow}|^2 + |\psi_{\downarrow\downarrow}|^2$ .

At  $\alpha = 0$ ,  $H_{c,v}$  in Eq. (3) becomes diagonal, allowing us to classify excitons by  $s_{v(c)}$ , the principal  $n$  and angular quantum numbers  $m$  ( $1s, 2s, 2p_{\pm}$  etc) [37, 38], the corresponding energies and wave functions, are given by

$$\begin{aligned} \Omega_{n,m;s_v s_c}^0 &= 2\Delta - s_v^v \Delta_v + s_c^c \Delta_c + E_{n,m}, \\ \vec{\Psi}_{n,m;s_v s_c}^0(\mathbf{r}) &= e^{im\phi} \mathcal{R}_{n,m}(r) |s_v, s_c\rangle, \end{aligned} \quad (5)$$

where  $\mathbf{r} = (r, \phi)$ ,  $\mathcal{R}_{n,m}(r)$  is the radial part of the wave function,  $E_{n,m}$  is the binding energy, and  $s_z^{c,v} = \pm 1$ . Both  $\mathcal{R}_{n,m}$  and  $E_{n,m}$  depend on  $V(r)$ : For  $V(r) \propto 1/r^2$ , we have the 2D Rydberg series  $E_{n,m} = -R_y / (n + 1/2)^2$ . A more accurate Rytova-Kelydish potential [39, 40] gives  $m$ -dependent  $E_{n,m}$ . For  $s$  states ( $m = 0$ ),  $\mathcal{R}_{n,0}(r \rightarrow 0) \neq 0$ . Other excitons ( $m \neq 0$ ) have  $\mathcal{R}_{n,m \neq 0}(r \rightarrow 0) = 0$ . Therefore, the matrix element from Eq. (4) can be nonzero only for  $s$  excitons, suggesting that  $2p$ -excitons are dark.  $\mathcal{R}_{1s}(r \rightarrow 0) \gg \mathcal{R}_{2s}(r \rightarrow 0)$  and the 2D absorption spectrum is dominated by the  $1s$  excitons.

With  $\alpha \neq 0$  due to the broken mirror symmetry,  $(n, m, s_v, s_c)$  are no longer good quantum numbers:  $H$  from Eq. (3) commutes only with the operator of the total angular momentum defined as

$$\hat{J}_z = -i\partial_{\phi} - (1/2)I \otimes \sigma_z + (1/2)\sigma_z \otimes I, \quad (6)$$

and a proper classification of excitonic states is based on the eigenvalues of  $\hat{J}_z$ , denoted by integer  $l$ . We assume a weak intersubband coupling compared to the energy gap and the Coulomb interaction. Treating  $\alpha$  as a perturbation, the exciton wave function  $\vec{\Psi}_l(\mathbf{r})$  can be expressed in terms of unperturbed states  $\vec{\Psi}_{n,m;s_v s_c}^0$  from Eq. (5)

$$\vec{\Psi}_l(\mathbf{r}) = \begin{pmatrix} c_{\uparrow\uparrow} \mathcal{R}_{n_{\uparrow\uparrow},l}(r) \\ c_{\uparrow\downarrow} \mathcal{R}_{n_{\uparrow\downarrow},l+1}(r) e^{i\phi} \\ c_{\downarrow\uparrow} \mathcal{R}_{n_{\downarrow\uparrow},l-1}(r) e^{-i\phi} \\ c_{\downarrow\downarrow} \mathcal{R}_{n_{\downarrow\downarrow},l}(r) \end{pmatrix} e^{il\phi}, \quad (7)$$

where  $n_{s_v s_c}$  is the principal quantum number of the  $|s_v s_c\rangle$  state, and the coefficients  $c_{s_v s_c}$  should be determined from the secular equation.  $\vec{\Psi}_l(\mathbf{r})$  displays the mixing between states with different  $l$  and subband indices.

The  $s-p$  mixing is realized at  $l = 0$  with the most efficient brightening of spin-forbidden  $2p$  excitons. The mixing strength is inversely proportional to energy difference between the spin forbidden  $2p$  state and spin allowed  $1s$  states. For example, the exciton in the state  $|2p_{+\uparrow\downarrow}\rangle$  with  $\vec{\Psi}_{2p_{+\uparrow\downarrow}}^0 = \mathcal{R}_{2p_+}(r) e^{i\phi} |\uparrow\downarrow\rangle$  gets an admixture,  $\delta \vec{\Psi}_{2p_{+\uparrow\downarrow}}$ , consisting of  $|1s_{\uparrow\uparrow}\rangle$  and  $|1s_{\downarrow\downarrow}\rangle$

$$\delta \vec{\Psi}_{2p_+} = -i\alpha I_{sp} \left( \frac{\Psi_{1s_{\uparrow\uparrow}}^0}{\Delta_{sp} - 2\Delta_c} + \frac{\Psi_{1s_{\downarrow\downarrow}}^0}{\Delta_{sp} - 2\Delta_v} \right), \quad (8)$$

where  $I_{sp} = 2\pi \int r dr \mathcal{R}_{1s}(r)[\partial_r \mathcal{R}_{2p}(r) + \mathcal{R}_{2p}(r)]$ , and Eq. (5) is used to calculate exciton energy differences.  $s-p$  mixing yields a partial brightening of  $2p_+$  exciton: the matrix element from Eq. (4) scales as  $\propto \alpha v_F I_{sp} \mathcal{R}_{1s}(0)$  at a fixed  $\Delta_{c(v)}$ . With a tunable  $\Delta_{c(v)}$ , we consider  $|2\Delta_{c(v)}| = \Delta_{sp}$  for a resonant condition of  $\Omega_{2p_+\uparrow\downarrow}^0 = \Omega_{1s\uparrow}^0$  or  $\Omega_{1s\downarrow}^0$ . The denominators in Eq. (8) diverge, one has to solve a full secular equation for  $c_{s_v s_c}$ .

To confirm these predictions and accurately include the Coulomb interaction in the absorption spectra, we use the BSE where the state  $|S\rangle$  exciton is expressed as a many-body wave function built from the eigenstates of the single-particle  $H$  from Eq. (1), as  $|S\rangle = \sum_{v\mathbf{c}\mathbf{k}} \mathcal{A}_{vc}^S(\mathbf{k}) |v\mathbf{c}\mathbf{k}\rangle$ , with  $|v\mathbf{c}\mathbf{k}\rangle = \hat{c}_{\mathbf{c}\mathbf{k}}^\dagger \hat{c}_{v\mathbf{k}} |0\rangle$ , where the ground state,  $|0\rangle$ , consists of fully occupied  $v$  bands and empty  $c$  bands,  $c_{\mathbf{c}\mathbf{k}}^\dagger$  ( $c_{v\mathbf{k}}$ ) is the creation (annihilation) of an electron in the eigenstate  $|c_\pm, \mathbf{k}\rangle$ ,  $|v_\pm, \mathbf{k}\rangle$  of  $H$ , where  $c_\pm, v_\pm$  are subband indices. The exciton envelope wave function in  $k$ -space,  $\mathcal{A}_{vc}^S(\mathbf{k})$ , and the corresponding exciton energy,  $\Omega^S$ , are calculated by solving the BSE [1, 13]

$$\begin{aligned} \Omega_S \mathcal{A}_{vc}^S(\mathbf{k}) &= [\epsilon_c(\mathbf{k}) - \epsilon_v(\mathbf{k})] \mathcal{A}_{vc}^S(\mathbf{k}) \\ &- \frac{1}{A} \sum_{v'\mathbf{c}'\mathbf{k}'} V(|\mathbf{k} - \mathbf{k}'|) \langle c\mathbf{k} | c'\mathbf{k}' \rangle \langle v'\mathbf{k}' | v\mathbf{k} \rangle \mathcal{A}_{v'\mathbf{c}'}^S(\mathbf{k}'), \end{aligned} \quad (9)$$

where  $\epsilon_{c,v}(\mathbf{k})$  are the single particle energies of  $H$ ,  $V(|\mathbf{k} - \mathbf{k}'|)$  is the Fourier component of the screened Coulomb interaction,  $A$  is the area of our system.

Using  $\vec{\mathcal{A}}^S(\mathbf{k}) = [\mathcal{A}_{++}^S(\mathbf{k}), \mathcal{A}_{+-}^S(\mathbf{k}), \mathcal{A}_{-+}^S(\mathbf{k}), \mathcal{A}_{--}^S(\mathbf{k})]^T$ , we can relate  $\vec{\mathcal{A}}^S(\mathbf{k})$  to  $\vec{\Psi}_l(\mathbf{r})$  from Eq. (7) by performing the Fourier and unitary transformations (changing the basis from  $|s_v, s_c\rangle$  to  $|v\mathbf{c}\mathbf{k}\rangle$ ), allowing us to express

$$\vec{\mathcal{A}}_l(\mathbf{k}) = \begin{pmatrix} Q_{++}(k) \\ Q_{+-}(k)e^{i\phi_k} \\ Q_{-+}(k)e^{-i\phi_k} \\ Q_{--}(k) \end{pmatrix} e^{il\phi_k}, \quad (10)$$

with  $\mathbf{k} = (k, \phi_k)$ , and the functions  $Q_{vc}$  can be expressed through  $R$ , see [36]. Generally,  $Q_{vc}$  is an admixture of all 4 components of  $\vec{\Psi}_l$ . Only in the limit of  $\alpha k \ll \Delta_{c,v}$ , when the basis  $|v\mathbf{c}\mathbf{k}\rangle \approx |s_v s_c\rangle$ ,  $Q_{vc}$  becomes determined by the Fourier transform of the single component  $\mathcal{R}_{nm}$ . For each component of  $\vec{\mathcal{A}}^S(\mathbf{k})$ , we can define the winding number,  $w$ , which counts the number of times the phase in  $\mathcal{A}_{vc}^S(\mathbf{k})$  rotates when completing a full circle in  $\phi_k$  [41, 42]. We note that,  $\mathcal{A}_{vc}^S(\mathbf{k})$  is gauge-dependent, a gauge consistent with our analytical EMA method is used [36].

The absorption coefficient of photon  $\sigma_\pm$  at angular frequency  $\omega$  is evaluated from

$$\alpha^\pm(\omega) = \frac{4e^2\pi^2}{c\omega} \sum_S |\langle S | \sigma_\pm | 0 \rangle|^2 \delta(\hbar\omega - \Omega^S), \quad (11)$$

where  $\langle S | \sigma_\pm | 0 \rangle = \sum_{v\mathbf{c}\mathbf{k}} [\mathcal{A}_{vc}^S(\mathbf{k})]^* \mathcal{D}_{vc}(\mathbf{k}) / A$ . The optical transition matrix element is  $\mathcal{D}_{vc}^\pm(\mathbf{k}) = \langle c\mathbf{k} | \hat{v}_\pm | v\mathbf{k} \rangle$ , with

$\hat{v}_\pm = (\hat{v}_x \pm i\hat{v}_y) / \sqrt{2}$ , and  $\hat{v}_{x,y} = \partial H_0 / \partial (\hbar k_{x,y})$ . To fit the absorption with experiments, we replace the  $\delta$ -function by a Lorentzian of a finite spectral width,  $\Gamma = 5$  meV.

We first consider magnetically proximitized ML-TMDs. We use an out-of-plane orientation of the substrate magnetization, with spin-subband splittings:  $\Delta_{c(v)} = \lambda_{c(v)} - J_{c(v)}$ , where  $\lambda_{c(v)}$  and  $J_{c(v)}$  are the intrinsic SOC and the exchange splitting due to the magnetic proximity effect in  $c(v)$  bands of ML-TMDs. Typically,  $\lambda_v$  of a few hundred meV exceeds greatly  $\lambda_c, J_c$ .  $\Delta_v \gg \Delta_c$  implies the formation of exciton series  $A$  and  $B$  related to spin states  $v = |\uparrow\rangle$  and  $|\downarrow\rangle$  and separated by the energy  $\Delta_v$ . This allows us to consider the  $s-p$  mixing within the  $A$ - and  $B$ -series independently, neglecting the  $A$ - $B$  coupling effects [the first two and the last two components are considered independently in Eq. (7)]. The resonant condition for the  $s-p$  mixing is then realized by varying  $\Delta_c$  through  $J_c$ . The substrate-induced breaking of the mirror symmetry also leads to the Rashba SOC, providing the spin-subband coupling needed for  $s-p$  mixing. The Rashba SOC takes the form  $\gamma \rightarrow i\gamma_R$  in Eq. (1), corresponding to  $\pm\alpha(k_x\sigma_y - k_y\sigma_x)$  in  $H_{c(v)}$ , Eq. (2), with  $\alpha \rightarrow i\alpha_R$ . The SOC-strength  $\alpha_R \sim 0.15$  eVÅ.

In Fig. 2 we show the calculated absorption as the function of frequency and the proximity-induced exchange

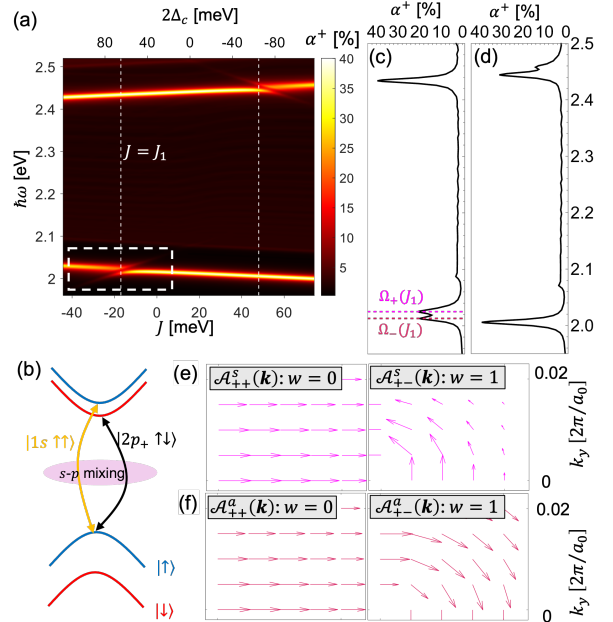


FIG. 2. BSE results for ML-TMD: (a) Brightening of the  $|2p_+\uparrow\downarrow\rangle$  and  $|2p_-\downarrow\uparrow\rangle$  excitons with different  $J$ . Anticrossings appear in lower-left [its enhanced view, white rectangle, in Fig. 2(b)] and upper-right region. (b) Mixing of the  $|1s\uparrow\uparrow\rangle$  and  $|2p_+\uparrow\downarrow\rangle$  excitonic states. (c), (d) The absorption spectra at two  $s-p$  resonances. Marked as vertical white dashed lines in (a). (e), (f) Phases of dominant components of  $\vec{\mathcal{A}}^{s,a}(\mathbf{k})$ , see Eq. (14). The direction (length) of an arrow denotes the phase and (the magnitude). Exciton energies at the resonance and their evolution with  $J$  are marked in (c) and Fig. 1(b).

interaction,  $J$ , with  $J_c = J$ ,  $J_v = 0.76J$ , guided by  $\text{WSe}_2/\text{EuS}$  parameters [36]. The absorption is dominated by two resonant lines of  $A:1s$  ( $\hbar\omega \approx 2.02$  eV) and  $B:1s$  ( $\hbar\omega \approx 2.43$  eV) excitonic transitions, showing a linear slope  $\pm 0.24$  with  $J$ . The anticrossings from the  $s-p$  resonances are at  $2\Delta_c = \pm\Delta_{sp} = \pm 65$  meV for  $A$  or  $B$  exciton series. The resonant absorption spectrum has a double-peak frequency profile, shown in Figs. 2(c), 2(d).

To further clarify the obtained resonant  $s-p$  mixing, we focus on  $A$ -excitons (negative  $J_c$ , see Fig. 1), and ignore a weak admixture of  $B$ -exciton states. With the basis  $|1s\uparrow\uparrow\rangle$  and  $|2p_+\uparrow\downarrow\rangle$ , the effective Hamiltonian is

$$H_{\text{ML}} = \begin{pmatrix} \Omega_{\uparrow\uparrow 1s}^0 & \alpha_R I_{sp} \\ \alpha_R I_{sp} & \Omega_{\uparrow\downarrow 2p_+}^0 \end{pmatrix}, \quad (12)$$

giving us the energies  $\Omega_{\pm} = \bar{\Omega} \pm \sqrt{(\Delta_{\Omega})^2 + (\alpha_R I_{sp})^2}$ , where  $\bar{\Omega} = [\Omega_{\uparrow\uparrow 1s}^0 + \Omega_{\uparrow\downarrow 2p_+}^0]/2$ , and the detuning is  $\Delta_{\Omega} = (\Omega_{\uparrow\uparrow 1s}^0 - \Omega_{\uparrow\downarrow 2p_+}^0)/2$ . The energies,  $\Omega_{\pm}$ , shown in Fig. 1(b) with dashed black lines as a function of  $J$  or  $2\Delta_c$ , feature the anticrossing and are in agreement with the exact absorption obtained from BSE in Fig. 1(b).

At the resonance,  $\Delta_{\Omega} = 0$ , we have  $\Omega_{\pm} = \bar{\Omega} \pm \alpha_R I_{sp}$ , with the energy splitting,  $\delta\Omega = 2\alpha_R I_{sp}$ , proportional to  $\alpha_R$  and the eigenstates given by the symmetric (s) and antisymmetric (a) combinations of  $|1s\uparrow\uparrow\rangle$  and  $|2p_+\uparrow\downarrow\rangle$

$$\Psi_{s,a} = \left( \Psi_{1s\uparrow\uparrow}^0(r) \pm \Psi_{2p_+\uparrow\downarrow}^0 \right) / \sqrt{2}. \quad (13)$$

We estimate  $\delta\Omega \approx 16$  meV, defining the typical beating frequency between the states s/a. The oscillator strength becomes equally distributed between two peaks separated by  $\delta\Omega$ , shown in Figs. 2(a), 2(c). To observe the double peak structure in absorption, as in Fig. 2(c), one needs to cool sample to suppress the exciton broadening,  $\Gamma \lesssim \delta\Omega$ .

It is instructive to discuss the exciton eigenstates Eq. (13) in the BSE form

$$\vec{\mathcal{A}}^{s,a}(\mathbf{k}) = [\mathcal{Q}_{++}^{s,a}(\mathbf{k}), \mathcal{Q}_{+-}^{s,a}(\mathbf{k})e^{i\phi_{\mathbf{k}}}, 0, 0]^T. \quad (14)$$

The winding number structure of  $\vec{\mathcal{A}}^{s,a}(\mathbf{k})$  is confirmed from BSE, as shown in Figs. 2(e), 2(f), with the winding numbers  $w = 0, 1$ . The last two components are zero, since contributions from  $B$ -excitons are negligibly small. The resonant character of the  $s-p$  mixing is not explicitly accessible in  $\mathcal{Q}^{s,a}$ , which complicates the analysis of this effect in 2D materials only from the BSE method. The actual  $k$ -dependence of  $\mathcal{Q}(k)$  does not display signatures of s/a structures from Eq. (13) due to a large spread of the 2D exciton wave function in  $k$ -space with  $\alpha k_{ex} \gtrsim \Delta_c$ , where  $k_{ex}$  is the  $k$ -space exciton Bohr radius.

We next consider  $H$  which retains the electron-hole and the subband symmetry ( $\Delta_c = \Delta_v$ ). This can be realized in a spinless model of 3R-stacked BL-TMD, where only the lower(upper)  $c(v)$  bands of the t and b layers are taken into account. Here our spinor notation  $|\uparrow(\downarrow)\rangle$  denotes t(b) layer states, shown in Fig. 3. The symmetric subband splittings are controlled by an out-of-plane

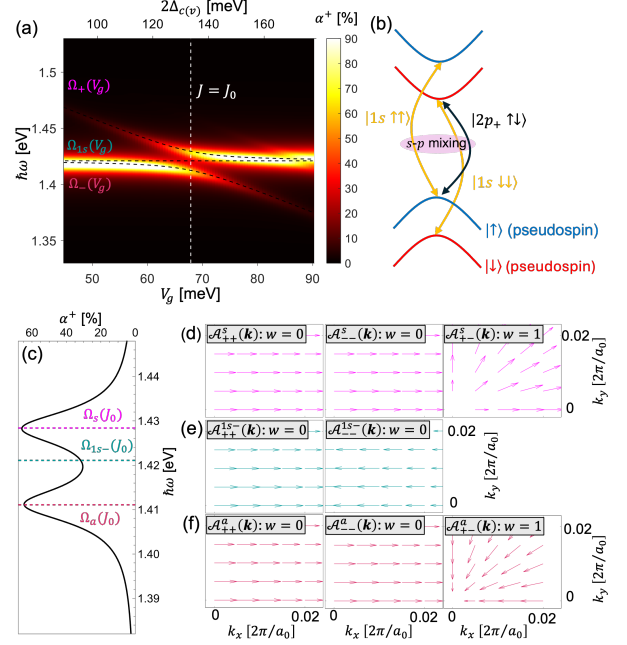


FIG. 3. BSE results for 3R stacked BL-TMD: (a) Evolution of the absorption as the subband splitting  $2\Delta_{c(v)}$  is tuned through out-of-plane gate voltage  $V_g$ . (b) Mixing of the intralayer  $1s$  excitons and the interlayer  $|2p_+\uparrow\downarrow\rangle$  exciton. The  $|\uparrow(\downarrow)\rangle$  pseudospin denotes the t(b) layer index. (c) The absorption line at the resonance, as marked by the white dashed line in (a). (d)-(f). Phases of the dominant components of  $\vec{\mathcal{A}}^{s,a}(\mathbf{k})$  and  $\vec{\mathcal{A}}^{1s-}(\mathbf{k})$ . Corresponding exciton energies at the resonance and evolution with  $V_g$  are marked in (c) and (a).

gate voltage  $V_g$ , following  $2\Delta_{c(v)} = V_g$ . The mixing is realized due to an interlayer coupling described by real  $\gamma$  in  $H$ , which gives the Dirac term  $\pm\alpha_I(k_x\sigma_x + k_y\sigma_y)$ , with  $\alpha \rightarrow \alpha_I$  in the downfolded  $H_{c(v)}$  from Eq. (2).

In this case, the exciton energies in the  $|\uparrow\uparrow\rangle$  and  $|\downarrow\downarrow\rangle$  series are the same, suggesting the use of the basis  $|\eta_{\pm}\rangle = (|\uparrow\uparrow\rangle \pm |\downarrow\downarrow\rangle) / \sqrt{2}$ . To identify the structure of the resonant  $s-p$  mixing, we write the effective Hamiltonian in the basis  $|1s\eta_{-}\rangle$ ,  $|1s\eta_{+}\rangle$  and  $|2p_+\uparrow\downarrow\rangle$

$$H_{BL} = \begin{pmatrix} \Omega_{1s\eta_{-}}^0 & 0 & 0 \\ 0 & \Omega_{1s\eta_{+}}^0 & -i\sqrt{2}\alpha_I I_{sp} \\ 0 & i\sqrt{2}\alpha_I I_{sp} & \Omega_{\uparrow\downarrow 2p_+}^0 \end{pmatrix}, \quad (15)$$

where  $\Omega_{1s\eta_{\pm}}^0 = \Omega_{1s\uparrow\uparrow}^0 = \Omega_{1s\downarrow\downarrow}^0$ . The lower block of Eq. (15) has the same form as Eq. (12). As a consequence, the absorption spectrum, the exciton energies evolution, and the winding numbers of  $\vec{\mathcal{A}}^{s,a}(\mathbf{k})$  are the same as in the previous case in Fig. 2. Unlike in ML-TMDs, we realize a dark spin-allowed  $1s$  exciton:  $|1s\eta_{-}\rangle$ . This exciton configuration consists of optically bright  $1s$  states but becomes completely dark because of its wave function anti-symmetrization, as in Eq. (4). The corresponding wave function anti-symmetrization is confirmed

in Fig. 3(e). The constant energy of this exciton is a straight horizontal line in Fig. 3(a) which lies between the two bright  $s-p$  mixed states. Despite an effective mixing between 3 exciton states, the calculated absorption displays only a single anticrossing feature accompanied by the formation of a double peak structure in its frequency profile, as shown in Fig. 3(c), making the picture qualitatively similar to the magnetically-proximitized TMDs with Rashba SOC in Fig. 1(b) and Fig. 2(a).

Our predictions have focused on the two specific examples of magnetically-proximitized monolayer TMDs and 3R-stacked bilayer TMDs. However, the principle of resonant mixing of excitonic states with different orbital symmetry can be extended to other materials systems, and have many further implications. With a small twisting angle in (nearly)commensurate bilayer TMDs an applied gate voltage may also brighten interlayer  $R_h^M$   $2p$  excitons, where the effective Hamiltonian can be written in the form of  $H_{BL}$  in Eq. (15) [2, 43, 44]. It would be instructive to consider resonant mixing in the recently found valley-dependent magnetic proximity effects [45], leading to an intriguing possibility of the topological effects and gap closing at only one (K or K') valley [46] and the resulting change of the helicity of the emitted light.

With the importance of Rashba spin-orbit coupling to the mechanism of spin-mixing, recently demonstrated to also dominate the spin relaxation of interlayer MoSe<sub>2</sub>/MoS<sub>2</sub> excitons [8], it would be helpful examine Janus TMDs [47] and generalize spin-orbit coupling beyond the usual  $k$ -linear dependence. There is a growing class of materials where its  $k$ -cubic dependence is signif-

icant and can alter the orbital symmetry of the proximity effects [48], while  $s-p$  mixing could be replaced by other orbital symmetry mixing. For these studies, our employed approach which combines the solutions of Bethe-Salpeter equation with the transparent symmetry analysis and massive Dirac electron model could also provide useful insights.

While the presence of  $s-p$  and mixing of other symmetries is more generic, the resonant character of the mixing and the associated anticrossing features have distinct and largely unexplored properties. This resonant mixing becomes possible since with a larger binding energy of excitons, due to the reduced screening of Coulomb interaction, there is also a larger  $1s$  to  $2p$  energy separation, close to the magnitude of the spin splitting in the conduction band. A challenge for future materials studies is to identify systems with an even larger and tunable spin splitting to match these two energies. From magnetic proximity effects, such experimentally realized spin splitting in TMDs is  $\sim 20$  meV [12, 15, 49], already much larger than what is feasible with the strongest applied magnetic field. Taken together, the excitonic signatures and resonant spin mixing in systems with tunable spin splitting can offer a sensitive probe for various forms of spin-orbit coupling as well design optical response in spintronic devices not limited to magnetoresistance [50–54].

*Acknowledgements.* We thank G. Xu and B. Scharf for valuable discussions. This work was supported by the U.S. Department of Energy, Office of Science, Basic Energy Sciences under Award No. DE-SC0004890. Computational resources were provided by the UB Center for Computational Research.

- 
- [1] G. Wang, A. Chernikov, M. M. Glazov, T. F. Heinz, X. Marie, T. Amand, and B. Urbaszek, Colloquium: Excitons in atomically thin transition metal dichalcogenides, *Rev. Mod. Phys.* **90**, 021001 (2018).
  - [2] D. Huang, J. Choi, C. Shih, and X. Li, Excitons in semiconductor moiré superlattices, *Nat. Nanotechnol.* **17**, 227 (2022).
  - [3] M. Syperek, R. Stühler, A. Consiglio, P. Holewa, P. Wyborski, L. Dusanowski, F. Reis, S. Höfling, R. Thomale, W. Hanke, R. Claessen, D. Di Sante, and C. Schneider, Observation of room temperature excitons in an atomically thin topological insulator, *Nat. Commun.* **13**, 6313 (2022).
  - [4] K. F. Mak and J. Shan, Photonics and optoelectronics of 2D semiconductor transition metal dichalcogenides, *Nat. Photon.* **10**, 216 (2016).
  - [5] D. Unuchek, A. Ciarrocchi, K. Watanabe, T. Taniguchi, and A. Kis, Room-temperature electrical control of exciton flux in a van der Waals heterostructure, *Nature* **560**, 340 (2018).
  - [6] D. Van Tuan, B. Scharf, Z. Wang, J. Shan, K. F. Mak, I. Žutić, and H. Dery, Probing many-body interactions in monolayer transition-metal dichalcogenides, *Phys. Rev. B* **99**, 085301 (2019).
  - [7] M. Grzeszczyk, S. Acharya, D. Pashov, Z. Chen, K. Vakinova, M. van Schilfgaarde, K. Watanabe, T. Taniguchi, K. S. Novoselov, M. I. Katsnelson, and M. Koperski, Strongly correlated exciton-magnetization system for optical spin pumping in CrBr<sub>3</sub> and CrI<sub>3</sub>, *Adv. Mater.* **35**, 2209513 (2023).
  - [8] H. Mittenzwey, A. M. Kumar, R. Dhingra, K. Watanabe, T. Taniguchi, C. Gahl, K. I. Bolotin, M. Selig, and A. Knorr, Ultrafast optical control of Rashba interactions in a TMDC heterostructure, *Phys. Rev. Lett.* **134**, 026901 (2025).
  - [9] Y. Shao, F. Dirnberger, S. Qiu, S. Acharya, S. Terres, E. J. Telford, D. Pashov, B. S. Y. Kim, F. L. Ruta, D. G. Chica, A. H. Dismukes, M. E. Ziebel, Y. Wang, J. Choe, Y. J. Bae, A. J. Millis, M. I. Katsnelson, K. Mosina, Z. Sofer, R. Huber, X. Zhu, X. Roy, M. van Schilfgaarde, A. Chernikov, and D. N. Basov, Magnetically confined surface and bulk excitons in a layered antiferromagnet, *Nat. Mater.* (2025).
  - [10] T. Galvani, F. Paleari, H. P. C. Miranda, A. Molina-Sánchez, L. Wirtz, S. Latil, H. Amara, and F. Ducastelle, Excitons in boron nitride single layer, *Phys. Rev. B* **94**, 125303 (2016).
  - [11] D. Xiao, G.-B. Liu, W. Feng, X. Xu, and W. Yao, Cou-

- pled spin and valley physics in monolayers of MoS<sub>2</sub> and other group-VI dichalcogenides, *Phys. Rev. Lett.* **108**, 196802 (2012).
- [12] I. Žutić, A. Matos-Abiague, B. Scharf, H. Dery, and K. Belashchenko, Proximitized materials, *Mater. Today* **22**, 85 (2019).
- [13] B. Scharf, G. Xu, A. Matos-Abiague, and I. Žutić, Magnetic proximity effects in transition-metal dichalcogenides: Converting excitons, *Phys. Rev. Lett.* **119**, 127403 (2017).
- [14] J. Joshi, B. Scharf, I. Mazin, S. Krylyuk, D. J. Campbell, J. Paglione, A. Davydov, I. Žutić, and P. M. Vora, Charge density wave activated excitons in TiSe<sub>2</sub>-MoSe<sub>2</sub> heterostructures, *APL Materials* **10**, 011103 (2022).
- [15] T. Norden, C. Zhao, P. Zhang, R. Sabirianov, A. Petrou, and H. Zeng, Giant valley splitting in monolayer WS<sub>2</sub> by magnetic proximity effect, *Nat. Commun.* **10**, 4163 (2019).
- [16] C. Serati de Brito, P. E. Faria Junior, T. S. Ghiasi, J. Ingla-Aynés, C. R. Rabahi, C. Cavalini, F. Dirnberger, S. Mañas-Valero, K. Watanabe, T. Taniguchi, K. Zollner, J. Fabian, C. Schüller, H. S. J. van der Zant, and Y. G. Gobato, Charge transfer and asymmetric coupling of MoSe<sub>2</sub> valleys to the magnetic order of CrSBr, *Nano Lett.* **23**, 11073 (2023).
- [17] D. Zhong, K. L. Seyler, X. Linpeng, N. P. Wilson, T. Taniguchi, K. Watanabe, M. A. McGuire, K.-M. C. Fu, D. Xiao, W. Yao, and X. Xu, Layer-resolved magnetic proximity effect in van der Waals heterostructures, *Nat. Nanotechnol.* **15**, 187 (2020).
- [18] X. Li, A. C. Jones, J. Choi, H. Zhao, V. Chandrasekaran, M. T. Pettes, A. Piryatinski, M. A. Tschudin, P. Reiser, D. A. Broadway, P. Maletinsky, N. Sinitsyn, S. A. Crooker, and H. Htoon, Proximity-induced chiral quantum light generation in strain-engineered WSe<sub>2</sub>/NiPS<sub>3</sub> heterostructures, *Nat. Mater.* **22**, 1311 (2023).
- [19] G. Xu, T. Zhou, B. Scharf, and I. Žutić, Optically probing tunable band topology in atomic monolayers, *Phys. Rev. Lett.* **125**, 157402 (2020).
- [20] P. E. Faria Junior and J. Fabian, Signatures of electric field and layer separation effects on the spin-valley physics of MoSe<sub>2</sub>/WSe<sub>2</sub> heterobilayers: From energy bands to dipolar excitons, *Nanomaterials* **13**, 1187 (2023).
- [21] F. Volmer, M. Ersfeld, P. E. Faria Junior, L. Waldecker, B. Parashar, L. Rathmann, S. Dubey, I. Cojocariu, V. Feyer, K. Watanabe, T. Taniguchi, C. M. Schneider, L. Plucinski, C. Stampfer, J. Fabian, and B. Beschoten, Twist angle dependent interlayer transfer of valley polarization from excitons to free charge carriers in WSe<sub>2</sub>/MoSe<sub>2</sub> heterobilayers, *npj 2D Mater. Appl.* **7**, 58 (2023).
- [22] Y. Wang, Z. Chen, X. Cheng, X. Su, P. Liu, F. Jia, R. Li, Y. Li, and G. Xu, Manipulation of optical response in transition metal dichalcogenides by magnetic proximity effects and strain, *Phys. Rev. B* **110**, 045425 (2024).
- [23] H. Yang, J. Zeng, Y. Shao, Y. Xu, X. Dai, and X.-Z. Li, Spin-triplet topological excitonic insulators in two-dimensional materials, *Phys. Rev. B* **109**, 075167 (2024).
- [24] B. S. D. Van Tuan, I. Žutić, and H. Dery, Marrying excitons and plasmons in monolayer transition-metal dichalcogenides, *Phys. Rev. X* **7**, 041040 (2017).
- [25] J. D. Cao, G. Xu, B. Scharf, K. Denisov, and I. Žutić, Emergent bright excitons with Rashba spin-orbit coupling in atomic monolayers, *Phys. Rev. B* **109**, 085407 (2024).
- [26] H. Dery and Y. Song, Polarization analysis of excitons in monolayer and bilayer transition-metal dichalcogenides, *Phys. Rev. B* **92**, 125431 (2015).
- [27] L. Chiroli, Brightening odd-parity excitons in transition-metal dichalcogenides: Rashba spin-orbit interaction, skyrmions, and cavity polaritons, *Phys. Rev. B* **101**, 075426 (2020).
- [28] M. M. Glazov, L. E. Golub, G. Wang, X. Marie, T. Amand, and B. Urbaszek, Intrinsic exciton-state mixing and nonlinear optical properties in transition metal dichalcogenide monolayers, *Phys. Rev. B* **95**, 035311 (2017).
- [29] B. Zhu, K. Xiao, S. Yang, K. Watanabe, T. Taniguchi, and X. Cui, In-plane electric-field-induced orbital hybridization of excitonic states in monolayer WSe<sub>2</sub>, *Phys. Rev. Lett.* **131**, 036901 (2023).
- [30] J. N. Engdahl, H. D. Scammell, D. K. Efimkin, and O. P. Sushkov, Excitons in atomically thin tmd in electric and magnetic fields, *arXiv:2409.18373*.
- [31] F. Zhang, C. S. Ong, J. W. Ruan, M. Wu, X. Q. Shi, Z. K. Tang, and S. G. Louie, Intervalley excitonic hybridization, optical selection rules, and imperfect circular dichroism in monolayer h-BN, *Phys. Rev. Lett.* **128**, 047402 (2022).
- [32] F. Bechstedt, *Many-Body Approach to Electronic Excitations* (Springer, 2016).
- [33] B. Scharf, D. V. Tuan, and I. Žutić, Dynamical screening in monolayer transition-metal dichalcogenides and its manifestations in the exciton spectrum, *J. Phys.: Cond. Matt.* **31**, 203001 (2019).
- [34] R. Winkler, *Spin-Orbit Coupling Effects in Two-Dimensional Electron and Hole Systems* (Springer, New York, 2003).
- [35] R. J. Elliott, Intensity of optical absorption by excitons, *Phys. Rev.* **108**, 1384 (1957).
- [36] See Supplemental Material for a discussion of the effective mass approximation and computational details.
- [37] X. L. Yang, S. H. Guo, F. T. Chan, K. W. Wong, and W. Y. Ching, Analytic solution of a two-dimensional hydrogen atom. I. Nonrelativistic theory, *Phys. Rev. A* **43**, 1186 (1991).
- [38] C. Y.-P. Chao and S. L. Chuang, Analytical and numerical solutions for a two-dimensional exciton in momentum space, *Phys. Rev. B* **43**, 6530 (1991).
- [39] N. S. Rytova, Screened potential of a point charge in a thin film, *Proc. MSU Phys.* **3**, 30 (1967).
- [40] L. V. Keldysh, Coulomb interaction in thin semiconductor and semimetal films, *JETP Lett.* **29**, 658 (1979).
- [41] X. Zhang, W.-Y. Shan, and D. Xiao, Optical selection rule of excitons in gapped chiral fermion systems, *Phys. Rev. Lett.* **120**, 077401 (2018).
- [42] T. Cao, M. Wu, and S. G. Louie, Unifying optical selection rules for excitons in two dimensions: Band topology and winding numbers, *Phys. Rev. Lett.* **120**, 087402 (2018).
- [43] F. Wu, T. Lovorn, and A. H. MacDonald, Theory of optical absorption by interlayer excitons in transition metal dichalcogenide heterobilayers, *Phys. Rev. B* **97**, 035306 (2018).
- [44] E. Regan, D. Wang, E. Paik, Y. Zeng, L. Zhang, J. Zhu, A. MacDonald, H. Deng, and F. Wang, Emerging exciton physics in transition metal dichalcogenide heterobilayers,

- Nat. Rev. Mater.* **7**, 778 (2022).
- [45] J. Choi, C. Lane, J.-X. Zhu, and S. A. Crooker, Asymmetric magnetic proximity interactions in MoSe<sub>2</sub>/CrBr<sub>3</sub> van der Waals heterostructures, *Nat. Mater.* **22**, 305 (2023).
- [46] T. Zhou and I. Žutić, Asymmetry in the magnetic neighbourhood, *Nat. Mater.* **22**, 284 (2023).
- [47] Z. Gan, I. Paradisanos, A. Estrada-Real, J. Picker, E. Najafidehaghani, F. Davies, C. Neumann, C. Robert, P. Wiecha, K. Watanabe, T. Taniguchi, X. Marie, J. Biskupek, M. Mundsziinger, R. Leiter, U. Kaiser, A. V. Krashennikov, B. Urbaszek, A. George, and A. Turchanin, Chemical vapor deposition of high-optical-quality large-area monolayer Janus transition metal dichalcogenides, *Adv. Mater.* **34**, 2205226 (2022).
- [48] M. Alidoust, C. Shen, and I. Žutić, Cubic spin-orbit coupling and anomalous Josephson effect in planar junctions, *Phys. Rev. B* **103**, L060503 (2021).
- [49] D. Wang and X. Zou, Tunable valley band and exciton splitting by interlayer orbital hybridization, *npj Comput. Mater.* **8**, 239 (2022).
- [50] J. Lee, S. Bearden, E. Wasner, and I. Žutić, Spin-lasers: From threshold reduction to large-signal analysis, *Appl. Phys. Lett.* **105**, 042411 (2014).
- [51] S. Liang, H. Yang, P. Renucci, B. Tao, P. Laczkowski, S. Mc-Murtry, G. Wang, X. Marie, J.-M. George, S. Petit-Watlot, A. Djeflal, S. Mangin, H. Jaffrès, and Y. Lu, Electrical spin injection and detection in molybdenum disulfide multilayer channel, *Nat. Commun.* **8**, 14947 (2017).
- [52] H. Tornatzky, C. Robert, P. Renucci, B. Han, T. Blon, B. Lassagne, G. Ballon, Y. Lu, T. Taniguchi, B. Urbaszek, J. M. J. Lopes, and X. Marie, Spin dependent charge transfer in MoSe<sub>2</sub>/hBN/Ni hybrid structures, *Appl. Phys. Lett.* **119**, 263103 (2021).
- [53] M. Lindemann, G. Xu, T. Pusch, R. Michalzik, M. R. Hofmann, I. Žutić, and N. C. Gerhardt, Ultrafast spin-lasers, *Nature* **568**, 212 (2019).
- [54] P. A. Dainone, N. F. Prestes, P. Renucci, A. Bouché, M. Morassi, X. Devaux, M. Lindemann, J.-M. George, H. Jaffrès, A. Lemaitre, X. B., M. Stoffel, T. Chen, L. Lombez, D. Lagarde, G. Cong, T. Ma, P. Pigeat, M. Vergnat, H. Rinnert, X. Marie, X. Han, S. Mangin, J.-C. Rojas-Sánchez, J.-P. Wang, N. C. Beard, I. Žutić, and Y. Lu, Controlling the helicity of light by electrical magnetization switching, *Nature* **627**, 783 (2024).